Journal of Asian Earth Sciences 73 (2013) 362–371

Contents lists available at SciVerse ScienceDirect

Journal of Asian Earth Sciences

journal homepage: www.elsevier.com/locate/jseaes

Origin of fluids in the Hetaoping Pb–Zn deposit, Baoshan–Narong–Dongzhi block metallogenic belt, Yunnan Province, SW China

Yulong Yang [a,b], Lin Ye [a,*], Zengtao Cheng [a,b], Tan Bao [a,b]

[a] State Key Laboratory of Ore Deposit Geochemistry, Institute of Geochemistry, Chinese Academy Sciences, Guiyang 550002, China
[b] Graduate University of Chinese Academy of Sciences, Beijing 100039, China

ARTICLE INFO

Article history:
Received 14 June 2012
Received in revised form 6 April 2013
Accepted 29 April 2013
Available online 13 May 2013

Keywords:
Baoshan–Narong–Dongzhi block metallogenic belt
Fluid inclusion
Ore-forming fluid
Concealed intrusion

ABSTRACT

The Hetaoping skarn type Pb–Zn deposit is located in the Baoshan–Narong–Dongzhi block metallogenic belt (BND belt), a belt between the Tengchong terrane and the Lanping basin. The deposit is hosted by marble of the upper Cambrian Hetaoping Formation and there are no outcrops of plutonic rocks present. This deposit is one of two large Pb–Zn deposits recently discovered in the BND belt. The Hetaoping deposit is a high Mn skarn. Four types of fluid inclusions were recognized in quartz from the deposit: vapor-rich inclusions (Type I), liquid-rich inclusions (Type II), pure vapor inclusions (Type III), and pure fluid inclusions (Type IV). The coexistence of Type I and Type III inclusions in Stage I (pre-ore stage) and Stage II (main ore stage) shows evidence of fluid boiling. Quartz-hosted fluid inclusions (Stage I and Stage II) display high homogenization temperatures and salinities (134–315 °C; 3.7–18.6 wt% NaCl equivalent) but calcite-hosted fluid inclusions in Stage III (post-ore stage) record lower homogenization temperatures and salinities (85–214 °C; 0.5–5.4 wt% NaCl equivalent). These data suggest a possible mixing between primary magmatic water and meteoric water. Based on chromatography data, the fluid inclusions in quartz contain abundant CO_2 and O_2 and subordinate CO, CH_4 and $C_2H_2 + C_2H_4$, suggesting an oxidizing environment. Based on their Na/K and Cl/SO_4 ratios, fluids contained in fluid inclusions are similar to volcanic spring waters. The low Na/K ratios (0.40–1.34) of the ore-forming fluids may have resulted from interaction with a deep alkaline intermediate-acid intrusion. Hydrogen and oxygen isotope determinations on quartz from different ore stages show low $\delta^{18}O$ and δD values relative to VSMOW (−4.3‰ to 2.3‰; −109‰ to −91‰), indicating that the ore-forming fluids were diluted by external fluid sources as the skarn system cooled. Overall, geological and geochemical interpretations suggest that the Hetaoping deposit is a distal manganese skarn Pb–Zn deposit related to concealed intrusions.

1. Introduction

The Hetaoping Pb–Zn deposit is one of two large Pb–Zn deposits explored recently in the Baoshan–Narong–Dongzhi block metallogenic belt (BND belt) (Fig. 1a). Most Pb–Zn skarn deposits occur near the contact zones between intrusions and predominantly carbonate-rich rocks (Meinert et al., 2005). Examples include the Phu Lon deposit, northern Loei Fold Belt, Thailand (Kamvong and Zaw, 2009), the Susurluk deposit, NW Turkey (Orhan et al., 2011), and the Nakatatsu deposit, Central Japan (Shimizu and Iiyama, 1982). However, some Pb–Zn skarns are hosted far from associated igneous rocks. The Hetaoping and other Pb–Zn deposits in the BND belt (e.g., Luziyuan) share some similar geological features with other skarn deposits like those noted above but they are of the second type just mentioned. In contrast to many skarn deposits the Hetaoping and Luziyuan deposits are hosted by marble with no associated igneous rocks.

Although quite a lot of work has been done on the ore deposits in the BND belt over the last decade, only a few geochemical studies on the origin and nature of the ore-forming fluids have be done (Chen et al., 2005; Xue et al., 2008, 2011).

The present study is an attempt to provide new insight into the nature and origin of the fluids that formed the Hetaoping deposit, using both existing and new fluid inclusions data and new hydrogen oxygen isotope data for vein quartz. The new fluid inclusion data include homogenization temperatures and salinity determinations from fluid inclusion in gangue quartz formed during different stages of ore formation. The present study demonstrates for the first time the existence of a lower Na/K and Cl/SO_4 end member fluid during Pb–Zn mineralization in the Hetaoping area. This end member fluid has important implications for the nature of the ore forming process.

2. Geological setting

The Hetaoping Pb–Zn deposit is a skarn deposit located 37 km north of Baoshan city, Yunnan Province, at latitude 25°25′24″ to

* Corresponding author. Tel.: +86 0851 5895591; fax: +86 0851 5891664.
E-mail address: yelin@vip.gyig.ac.cn (L. Ye).

1367-9120/$ - see front matter © 2013 Elsevier Ltd. All rights reserved.
http://dx.doi.org/10.1016/j.jseaes.2013.04.036

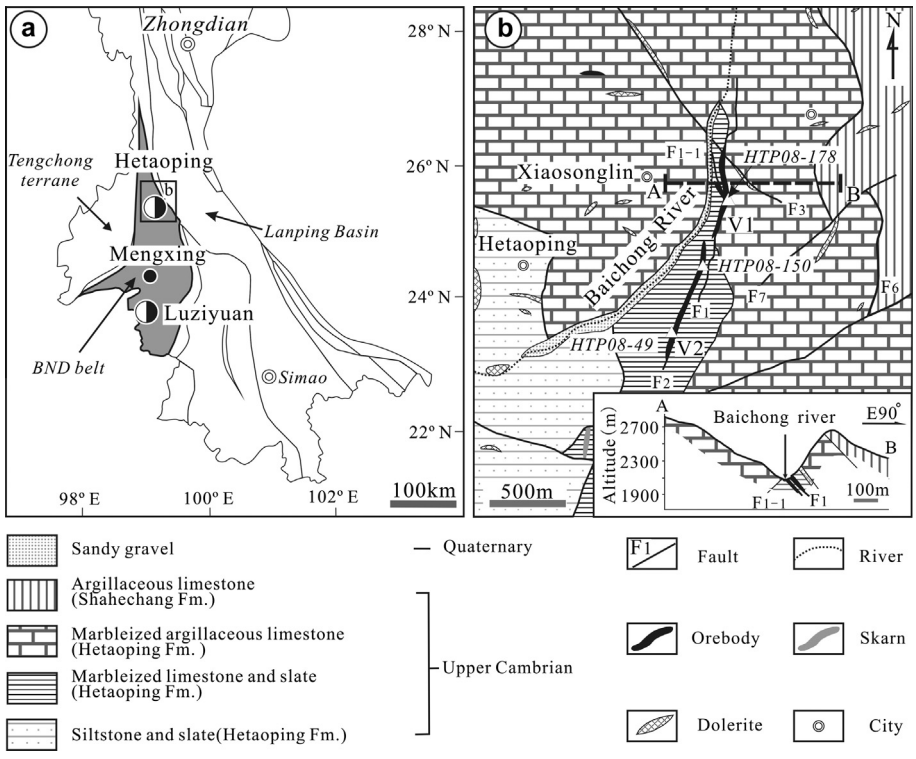

Fig. 1. (a) Regional geological map showing the location of the Hetaoping district (simplified from Ye et al., 2011). (b) Simplified geologic map of the Hetaoping deposit showing the distribution of rock units and the location of the ore bodies. The small box in (a) shows the location of (b). BND belt = Baoshan–Narong–Dongzhi block metallogenic belt.

25°27′34″N, longitude 99°08′21″ to 99°10′08″E. It is between at 2108 and 2696 m above sea level. Geologically it occurs in the BND belt of the Dian–Tai–Ma block metallogenic Province (Fig. 1a). The BND belt, between the Tengchong terrane and Lanping basin, hosts a number of large polymetallic deposits (Fig. 1a), such as the Luziyuan skarn type Pb–Zn deposit, the Dongshan hydrothermal type Pb–Zn deposit, the Mengxing MVT type Pb–Zn deposit, the Bawdwin VHMS Pb–Zn–Ag polymetallic deposit and the Hetaoping Pb–Zn skarn. These deposits have been described previously by a number of authors (Chen et al., 2009, 2005; Dong, 2007; Dong and Chen, 2007; Li et al., 1985, 2006; Xia et al., 2005; Xue et al., 2008, 2011; Zhu et al., 2006; Zaw, 2003). Although the Pb, Zn, Ag, Sn, and W polymetallic mineralization and skarns in the BND belt are attributed to granitoid magmatism in late-Yanshanian (Rao, 2008), at present no granitoid intrusions are exposed in the Baoshan block. However, data from geophysical exploration (Li and Mo, 2001) indicate that granitoid intrusions are present beneath the northern and southern portions of the BND belt (the Hetaoping and Luziyuan deposit areas, respectively). Based on stable and lead isotope data from the Hetaoping V1 ore body. Xue et al. (2008, 2011) have concluded that the ore-forming fluids that produced the deposits in the Hetaoping district are related to this intrusion.

The exposed units in the Hetaoping ore district are dominated by Upper Cambrian rocks including argillites of the Shahechang Formation and marbleized argillaceous limestone, marbleized limestone, slate, and siltstone of Hetaoping Formation. Carbonates predominate. The deposit has an average combined Pb + Zn grade of 5–11% and consists of three ore bodies, V1, V2 and V3 each of which can be variously stratiform, stratoid, lenticular or formed by veins. The V1 ore body, the largest, is 590 m long and 30 m wide (Xue et al., 2008; Zhu et al., 2006). It is controlled by a north–northeast-striking fault and hosted in marble of the Upper Cambrian Hetaoping Formation (Fig. 1b). The V1 orebody is the only one of the three investigated by this study. There is little outcropping igneous rock in the entire district except for sporadic diabase dikes which follow north–south, NW–SE, and NE–SW structural trends. The dikes range from several meters to several hundred meters in length and from several centimeters to several meters in width. The V1 ore body is cut by diabase dikes, indicating that the dikes are younger than the ore. The Yanshanian Zhibenshan granite (126.7 ± 1.6 Ma, Tao et al., 2010) and Yunlong granite (Zhang, 1990) are present northwest of the Hetaoping ore district.

Skarnification, pyritization, silicification and calcitization all occur extensively in the marble host rocks but skarnification is the most important type of alteration. The skarn mineral assemblages include garnet, diopside and hydrous minerals (e.g., epidote, actinolite, tremolite, Xue et al., 2011). These skarn minerals are zoned away from the Pb–Zn ore bodies in the following sequence: diopside–johannsenite-minor garnet → tremolite–actinolite → chlorite (Fig. 2). Xue et al. (2011) classify the skarn minerals as belonging to a manganiferous skarn assemblage. Dominant ore minerals in the deposit are sphalerite, galena, pyrite, chalcopyrite with minor magnetite, bornite, cubanite and marcasite, as well as cerusite, smithsonite and some oxidize minerals (e.g. willemite, greenockite, malachite). The sulfides are characterized by a high Mn content. Based on laser-ablation ICP mass-spectroscopy, sphalerite can contain up to 5766 ppm Mn (Ye et al., 2011). Overall, gangue minerals are mainly garnet, diopside, hedenbergite, ilvaite, actinolite, hopfnerite, epidote, chlorite, quartz, calcite, barite and fluorite. We have subdivided this gross mineralogy into subsets based on paragenesis. The simplified paragenetic sequences are:

Stage I (pre-ore): quartz–pyrite–chalcopyrite–Fe–sphalerite;
Stage II (the main ore stage): quartz–sphalerite–galena–chalcopyrite;
Stage III (post-ore): quartz–calcite.

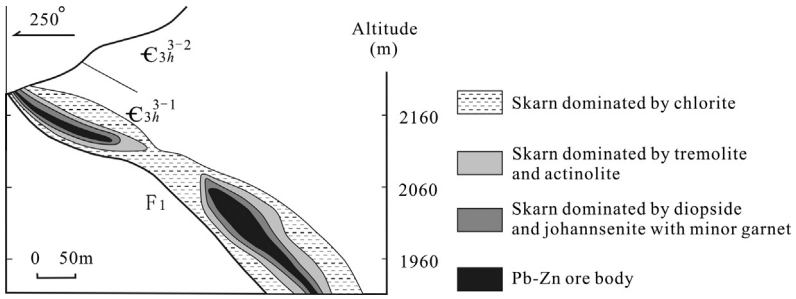

Fig. 2. Alteration zones around Hetaoping Pb–Zn skarn (simplified from Li et al., 2011).

3. Sampling and methodology

We collected ten samples representing three different types of sulfide ores from the Hetaoping V1 ore body: (1) 1-massive sulfide ores (samples HTP08-8, HTP08-11, HTP08-79, HTP08-93, HTP08-100, HTP08-115, HTP08-150 and HTP08-157), (2) disseminated sulfide ores (HTP08-177), and (3) veinlet sulfide ore (HTP08-178). Four samples of the host Hetaoping formation related to skarn were also sampled in order to have a representative sample of the early mineralization (samples HTP08-14, HTP08-49, HTP08-52 and HTP08-114). In addition, we also studied one quartz sample from the Heiyanao ore district (HYA08-14). These fifteen samples represent the three different stages of mineralization. Samples HTP08-14, HTP08-49, HTP08-52 and HTP08-114 of skarnified limestone represent mineralization from the pre-ore stage (Stage I), samples HTP08-8, HTP08-11, HTP08-79, HTP08-93, HTP08-100, HTP08-115, HTP08-150, HTP08-157, HTP08-177 and HTP08-178 from the Hetaoping V1 ore body represent the main ore stage (Stage II), and sample HYA08-14 represents an ore-free quartz vein in the post-ore-stage (Stage III). Fig. 1b shows a simplified geologic map of the Hetaoping deposit and the distribution of rock units and ore bodies.

3.1. Microthermometry and chromatography analyses

We performed microthermometry on inclusions from three different types of samples: (1) skarn (samples HTP08-49 and HTP08-114), (2) massive sulfide ores (HTP08-8, HTP08-79, HTP08-93, HTP08-150 and HTP08-157), and (3) a veinlet sulfide ore (HTP08-178). In addition, chromatography analyses were carried out on five different types of samples: (1) skarn (HTP08-14), (2) skarnoid (HTP08-52), (3) massive sulfide ores (HTP08-11, HTP08-115 and HTP08-100), (4) disseminated sulfide ore (HTP08-177), and (5) quartz vein (HYA08-14). Quartz was the mineral used for all fluid inclusions studies.

Microthermometry of fluid inclusions was conducted a Linkam THMSG-600 heating-freezing stage in the State Key laboratory of Ore Deposit Geochemistry, Chinese Academy of Sciences, Guiyang, China. The precision and accuracy of the microthermometry measurements, based on standard calibration procedures, was estimated to be ±2 °C during heating and ±0.1 °C during freezing. Salinity estimates were determined from the last melting temperature of ice (Bodnar, 1993).

To obtain material for fluid inclusion chromatography, purified quartz was isolated from quartz veins using standard separation techniques (elutriation and handpicking). Quartz was extracted from the 178 to 250 μm fraction and then placed into a 100 ml beaker containing chloroazotic acid and heated on a hotplate for 3 h at 80–90 °C. Residual acid adsorbed on the crystal surfaces and in intragranular defects was removed in an ultrasonic cleaner and the samples were then removed to a drying apparatus. In order to eliminate the influence of adsorbed water and air on N_2, O_2, CO, CO_2 and H_2O measurement, these gasses were driven off in a vacuum cylinder for 15 min at 100 °C. To collect sample material for the chromatography, the gas (containing H_2O, N_2, O_2, CO, CO_2, CH_4 and $C_2H_2 + C_2H_4$) an liquid (containing Ca^{2+}, K^+, Na^+, Mg^{2+}, Cl^-, SO_4^{2-}, F^-, NO_3^- and Br^-) were obtained the thermal decrepitation method in a furnace for 15 min at 500 °C. The gas and liquid compositions were measured at the Institute of Mineral Resources of the Chinese Academy of Geological Sciences, Beijing, China, using a GC2010 two-dimensional gas chromatograph and an HIC-SP super ion chromatograph made in Shimadzu Corporation, respectively. This method has been described by Yang et al. (2007). Analytical results are reported in mole fraction. The minimum detection limits for these data were 1 ppm for the gas and, for the liquid phases, 1 ppm for the cations and 1 ppb for the anions.

3.2. Hydrogen and oxygen isotope analyses

Selected samples of quartz from a skarnoid sample (HTP08-52), massive sulfide ores (samples HTP08-11 and HTP08-115), a disseminated sulfide ore sample (HTP08-177) and the quartz vein (HYA08-14) were analyzed for H and O isotopes. Coarse quartz was separated by handpicking using a binocular microscope, followed by repeated crushing and sieving. Samples were then washed in dehydrated ethanol to remove any impurities. Then hydrogen was extracted from a 4 to 8 g, 40 to 80 mesh size fraction and oxygen extracted from a 1 g, 200 mesh size fraction for isotope analysis. Hydrogen and oxygen isotope analyses were performed at the Key Laboratory of Isotopic Geology of the Ministry of Land and Resources, Beijing, China, using a MAT-253EM stable isotope mass spectrometer made in Finnigan corporation. The oxygen isotope composition of the samples was determined using the bromine pentafluoride method (Clayton and Mayeda, 1963). Samples for oxygen analysis were reacted with bromine pentafluoride for 15 h, and the O_2 gas produced was converted to CO_2 for mass spectrometric analysis though reaction with a graphite rod at 700 °C. The hydrogen isotope composition of the samples was measured using the closed tube technique described by Vennemann and O'Neil (1993). The quartz samples were heated in the closed tube to extract water and the obtained water was converted to H_2 by reaction with a Zn reagent. The obtained H_2 gas was frozen into a glass-tube containing activated carbon for mass spectrometric analysis. Analytical results are expressed in the standard per mil notation relative to VSMOW (Vienna Standard Mean Ocean Water) for oxygen (Craig, 1961; Baertschi, 1976) and hydrogen (Craig, 1961). Analytical precision was ±2‰.

4. Fluid inclusion studies

4.1. Fluid inclusion types and characteristics of fluid inclusion from different ore stages

We investigated fluid inclusions from the three different stages of ore formation and the textural relationship among these three different types of inclusions. Fluid inclusion origin was based on the criteria of Van den Kerkhof and Hein (2001). Although we probably studied some secondary inclusions owing to the lack of identifiable growth zones in the quartz crystals, the vast majority of the inclusions studied are presumed to be primary inclusions.

Four types of fluid inclusions in quartz were indentified in terms of the proportion of phases at room temperature: vapor-rich fluid inclusions (Type I), liquid-rich fluid inclusions (Type II), pure vapor fluid inclusions (Type III) and pure liquid fluid inclusions (Type IV). We observed Type II, Type IV and Type III inclusions in pre-ore stage samples (Fig. 3a-d). Type II and Type IV inclusions from 1 to 10 μm in size, occur abundantly both in closely spaced groups and as isolated positions. The larger inclusions generally occur as elliptical and negative crystal shapes whereas the smaller inclusions occur as elongated shapes. Type III inclusions, as well as Type II and Type IV, also occur together along healed cracks. All four types of fluid inclusions occur in the main ore stage (Fig. 3e–h), although we noted that the predominant types of inclusions in this stage are Types I and III. Type II inclusions are between 8 and 10 μm in size, have regular shapes and occur along with Type IV inclusions along at least two generations of healed fractures. In post-ore stage material, the majority of inclusions are Type II with fewer Type IV inclusions (Fig. 3i and j), and some of these inclusions, smaller than 4 μm in size, occur as abundant closely spaced inclusions along calcite crystal cleavage planes. We interpret these inclusions to be secondary. Secondary inclusions in quartz developed extensively during this entire stage, suggesting that fluid mixing may have occurred during the mineralization (Ahmad and Arthur, 1980).

4.2. Homogenization temperatures and salinity

Owing to their very small size, we were not able to collect microthermometric data from the post-ore stage inclusions. Thus, only fluid inclusions from the pre-ore stage and main ore stages were investigated. Table 1 is a summary of microthermometric data for the fluid inclusions in this study; chromatography data is summarized in Table 2.

Overall, quartz-hosted fluid inclusions record a broad range of homogenization temperatures, temperatures from 134 to 315 °C with an average value of 181 °C (n = 77); the data are concentrated toward the low end of that range (Fig. 4a). The salinities for these fluid inclusions range 3.7–18.6 wt% NaCl equivalent with an average value of 11.3 (n = 77). Most of the measured salinities are near the high end of the range. We found only two inclusions that recorded high temperatures namely 305 and 315 °C. Salinities for theses two inclusions were 10.2 and 15.8 NaCl equivalent, respectively (Fig. 4b). In addition, the microthermometric data show partly overlapping ranges in homogenization and last ice-melting temperatures among the three mineralization stages (Fig. 5). These data indicate that ore-forming fluids were a moderate to lower temperature fluids with lower to moderate salinities. It should be noted that homogenization temperatures for fluid inclusion in the main ore stage are greater than those for fluid inclusions in the other two stages. This observation is conformable with the larger number of Type I and Type III inclusions observed in the main ore stage samples and is consistent with separation of a vapor phase (Ahmad and Arthur, 1980; Wilkinson, 2001).

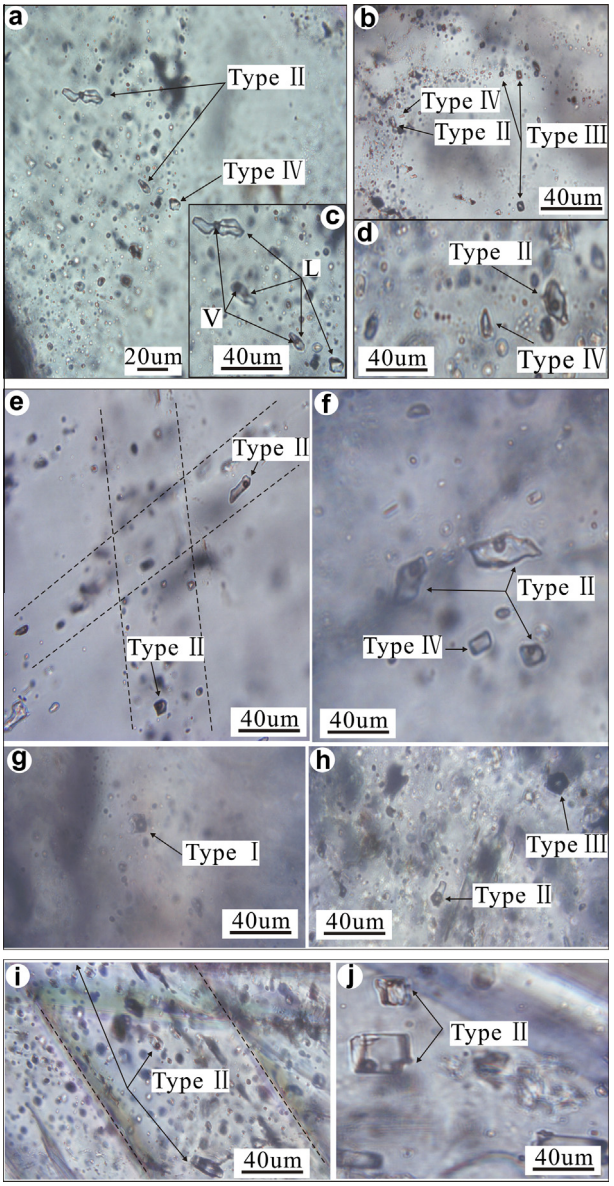

Fig. 3. Photomicrographs of fluid inclusions in quartz from the Hetaoping deposit. (a–d) Photomicrographs of Type II, Type III and Type IV fluid inclusions in quartz from the pre-ore stage. (e–h) Photomicrographs of Type I, Type II, Type III and Type IV fluid inclusions in quartz from the main ore stage. (i and j) Photomicrographs of Type II fluid inclusions in quartz from the post-ore stage.

The microthermometric data for fluid inclusions hosted by quartz that we have collected suggest that low-temperate and low-salinity ore-forming fluid were responsible for ore formation in the Hetaoping ore district.

4.3. Chromatography data

According to the bulk composition of the fluid inclusions from different stages (Table 2, Fig. 6a), the vapor phase composition of the fluid inclusions is mainly composed of H_2O with lesser amounts of CO_2, N_2 and O_2, and trace amounts of CO, CH_4, and $C_2H_2 + C_2H_4$. It is notable that oxidized species (CO_2 and O_2) are much more abundant than reduced species (CO, CH_4 and $C_2H_2 + C_2H_4$). This suggests that the ore-forming fluid evolved in an oxidizing environment. Both CO_2 and O_2 can be generated when permeating fluids interact with host rocks (Moura, 2008). N_2

Table 1
Summary of microthermometric characteristics for the fluid inclusions studied.

Sample type	Sample no.	Sample location	Studied lithologies	Host mineral	Mineralization stage	FI type	*n*	Homogenization *T* (°C)				Salinity (wt% NaCl equiv)			
								Min	Max	Std	Mean	Min	Max	Std	Mean
Skarn	HTP08-49	Hetaoping 36 # adit	Pyrite veinlet-rich quartz vein in retragrade skarn	Q1	I	Lv	16	151	192	12	170	3.7	17	3	14.6
Skarn	HTP08-114	Hetaoping 50 # adit	Dissemianted Pyrite-rich quartz and calcite vein in retragrade skarn			Lv	3	161	179	9.9	168	12	15	2	13.3
Massive sulfide ore	HTP08-79	Ore heap in Hetaopingmineral processing plant	Massive sphalerite ore and quartz vein	Q2	II	Lv	15	134	201	17	176	6.7	19	3	12
Massive sulfide ore	HTP08-93	Ore heap in Hetaoping mineral processing plant	Oxidized surface massive sphalerite ore and quartz vein			Lv	12	169	265	27	201	8.7	13	1	10.5
Massive sulfide ore	HTP08-150	Hetaoping 2048 adit in pit one	Sphalerite-rich massive sulfide ore with minor galena and quartz vein			Lv	7	165	305	47	206	8.3	14	2	10.9
Massive sulfide ore	HTP08-8	Hetaoping 88 # adit	Massive sphalerite ore with minor chalcopyrite in quartz vein			Lv	15	141	172	8.7	160	5.7	15	3	8.6
Massive sulfide ore	HTP08-157	Ore heap in Hetaoping mineral processing plant	Massive sphalerite–galena ore and quartz vein			Lv	7	156	315	57	214	6.9	16	3	9.5
Veinlet sulfide ore	HTP08-178	Ore heap in Hetaoping mineral processing plant	Sphalerite–galena rich quartz band in marbleized limestone			Lv	2	156	161	3.5	159	8.8	10	1	9.5
*				Cc	III	Lv	–	85	214		–	0.5	5.4		–

Q1 = Quartz from the first generation; Q2 = Quartz from the secondary generation; Lv = Liquid–vapor fluid inclusions. *-data from Chen et al. (2005).

Table 2
Chromatography data for the vapor phase and the liquid phase of selected fluid inclusions from Hetaoping.

Sample type	Sample no.	Sample location	Studied lithologies	Mineralization stage
Skarn	HTP08-14	Hetaoping 88 # adit	Pyrite–chalcopyrite quartz vein in retragrade skarn	I
Skarnoid	HTP08-52	Hetaoping 36 # adit	Banded sphalerite-rich sulfide ore with minor chalcopyrite and pyrite in skarnization limstone	I
Massive sulfide ore	HTP08-11	Hetaoping 88 # adit	Massive sphalerite–chalcopyrite ore and chalcopyrite rich quartz vein	II
Massive sulfide ore	HTP08-115	Hetaoping 50 # adit	Massive sphalerite and quartz vein	II
Disseminated sulfide ore	HTP08-177	Ore heap in Hetaoping mineral processing plant	Dissemianted sphalerite–galena ore and quartz vein in marbleized limestone	II
Massive sulfide ore	HTP08-100	Hetaoping 50 # adit	Massive sphalerite and quartz vein	II
Quartz vein	HYA08-14	1960 adit in Heniuao ore district	Quartz vein with no mineralization	III

Gas chromatograph data (mole fraction)								Ion chromatograph data (mole fraction)										
H_2O	CO_2	N_2	O_2	CO	CH_4	$C_2H_2 + C_2H_4$	C_2H_6	Ca^{2+}	K^+	Na^+	Mg^{2+}	Cl^-	SO_4^{2-}	F^-	NO_3^-	Br^-	Na/K	Cl/SO_4
84.74	9.35	4.18	3.06	1.21	0.05	0.01	nd	89.64	0.99	0.85	0	6.98	1.24	0.23	0.07	0	0.86	5.64
87.06	8.58	3.84	3.59	nd	0.04	0.01	nd	64.86	2.68	3.58	0.24	24.12	2.61	1.53	0.19	0.2	1.34	9.25
78.64	13.4	7.11	4.07	nd	0.03	0.01	nd	91.46	1.15	0.56	0	3.63	2.58	0.49	0.13	0	0.49	1.4
85.95	9.01	3.36	2.59	1.28	0.02	0.01	nd	94.82	0.3	0.13	0.03	0.73	0.41	3.55	0.02	0	0.43	1.81
91.54	5.78	2.31	2.65	nd	0.13	0.01	nd	91.1	1.85	0.75	0.15	4.31	1.7	0.08	0.05	0	0.41	2.53
82.53	11.9	3.8	0.32	1.31	0.08	0.03	0	0	6.58	2.63	1.34	31.68	54.07	2.2	0.88	0.62	0.4	0.59
82	12.2	5.25	3.04	nd	0.02	0.01	nd	89.75	2.09	1.26	0.71	2.7	3.26	0.22	0	0	0.6	0.83

content is noticeably higher during the entire ore stage (Table 2). Ore-stage N_2 content is 2.31–7.11 mol% with an average value of 5.24 mol%, suggesting that high N_2 fugacity may be a necessary condition for the formation of the Hetaoping deposit. In addition, the liquid phase of fluid inclusions is characterized by a high Cl^- and Ca^{2+} content and subordinate amounts of SO_4^{2-}, F^-, K^+, Na^+ and Mg^{2+} (Table 2, Fig. 6b). In addition some F-rich fluid inclusions in the pre-ore stage were observed, especially sample (HTP08-115) which had significant amounts of F (3.55 mol%). Xue et al. (2011) reported that fluid inclusions from Hetaoping ore contained elevated Na concentrations with only minor K present, however the fluid inclusions we analyzed displayed higher K values (mean 2.23 mol%) than Na values (mean 1.39 mol%). Our results show that ore-forming fluid in the Hetaoping ore district was a H_2O–CO_2–N_2–CaCl fluid.

5. Hydrogen and oxygen isotope studies

Hydrogen and oxygen isotope compositions of vein-quartz collected from skarnoid, massive sulfide ores, disseminated sulfide ores and a quartz vein are given in Table 3. The oxygen isotope

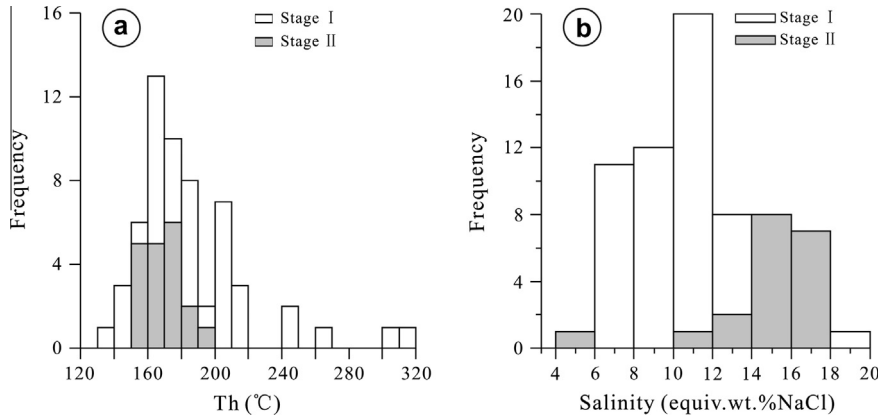

Fig. 4. Frequency histogram of homogenization temperatures (T_h) and salinities (equiv. wt% NaCl) for fluid inclusions from Stage I and Stage II.

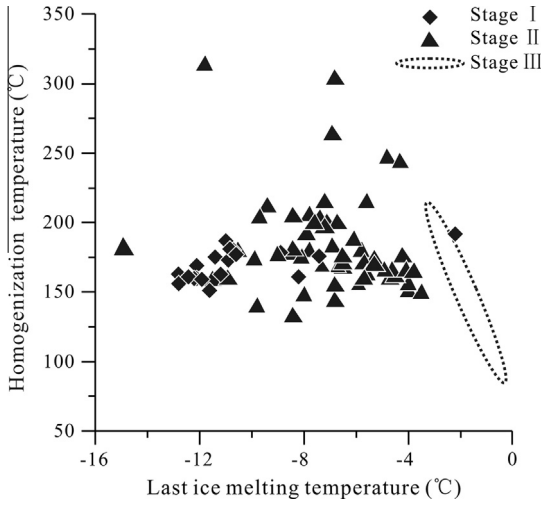

Fig. 5. Homogenization temperatures versus last-ice melting temperature (°C) for quartz-hosted fluid inclusions.

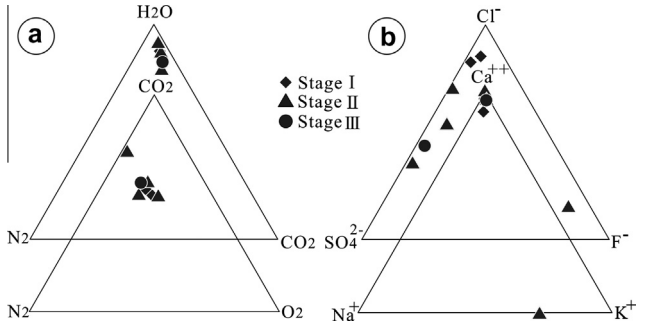

Fig. 6. Ternary diagrams, using mole values, for vapor phase composition (a) and liquid phase composition (b) of selected fluid inclusions from the three stages of ore formation at Hetaoping.

composition of fluids in equilibrium with quartz was calculated using appropriate fractionation factors (see footnote, Table 3). The $\delta^{18}O$ for quartz from the Hetaoping ore district ranges from 10.5‰ to 12.6‰ and is similar to that for quartz from another Mn-rich skarn deposits, the Bajiazi deposit in northeastern China. At Bajiazi, $\delta^{18}O$ for quartz is between 10.8‰ and 14.4‰ (Zhao et al., 2003). Compared to the isotopic composition of magmatic water ($\delta^{18}O$ = 6–10‰, δD = −50‰ to −80‰; Taylor, 1992), $\delta^{18}O$ and δD for fluids in equilibrium with Hetaoping quartz must have been significantly lower, down to $\delta^{18}O$ of −4.3‰ and δD of −109‰ respectively (Fig. 7). The low $\delta^{18}O_{fluid}$ and δD_{fluid} values may have been caused by dilution by a from an external fluid source (e.g., meteoric water). Note that the hydrogen isotope composition of the Hetaoping fluid is similar to that of present-day meteoric water (δD = −110‰ to −90‰; Xu and Mo, 2000).

6. Discussion

6.1. Comparison of Hetaoping fluid inclusion data from other deposits

The average and maximum homogenization temperatures and salinities recorded by quartz and calcite from Hetaoping are much lower than those from some other calcic–magnesian skarn deposits. Maximum temperatures and salinities at Hetaoping were 315 °C and 18.6 wt% NaCl. Values reported from other deposits include 350.9–468.5 °C and 0.5–23.1 wt% NaCl at Phu Lon, Thailand (Kamvong and Zaw, 2009), 312–470 °C and 5.9–63 wt% NaCl at Mazraeh, Ahar, NW Iran (Karimzadeh Somarin and Moayyed, 2002), 369 to >600 °C and 12–70 wt% NaCl at Susurluk, Turkey (Orhan et al., 2011), 145–500 °C and 1.2–13.0 wt% NaCl at Mengku, Xinjiang Altai, NW China (Xu et al., 2010) and 327–450 °C and 15–47.5 wt% NaCl at Bai Yinnuo, Neimong (Zhang et al., 1992). See Fig. 8. However, the fluids with lower homogenization temperatures and salinities are broadly analogous to fluids found in other manganese skarn orebodies from other parts of the world such as South Shaft, Argentina (Logan and Amelia, 2000) and Bajiazi (Zhao et al., 2003) and in hydrothermal type Pb–Zn deposit hosted in other parts of the BND belt like the Luziyuan deposits (Xia et al., 2005) and Jinchang (Chen et al., 2009) (Fig. 8). Manganiferous skarns in the Hetaoping ore district occur in the distal marbles and similar deposits have been studied in other area (Logan and Amelia, 2000; Meinert, 1987; Shimizu and Iiyama, 1982; Yun and Einaudi, 1982; Zhao et al., 2003). The studies from by Zhao (1997), Meinert (1987), and Meinert et al. (2005) have shown that manganese skarns generally form in the distal skarn zone whereas calcic–magnesian skarns formed in the proximal skarn zone. This is the reason Mn-skarn fluid inclusions homogenization temperatures are lower than those from Mg-skarn inclusions (200–450 °C versus 450–650 °C). These manganiferous skarns formed from lower temperature and lower salinity fluids. Based on their research of the Hetaoping ore district, Chen et al. (2005) and Zhu et al. (2006) have both concluded that the magnesian fluids involved in ore formation were derived predominantly from deep magmatic sources, sources first postulated by Allen and Fahey (1953). As stated above, we believe that the manganese-rich fluids responsible for

Table 3
Summary of hydrogen and oxygen isotope data for quartz from the Hetaoping deposit.

Sample type	Sample no.	Sample location	Studied lithologies	Mineral	$\delta D_{V\text{-}SMOW}$‰	$\delta^{18}O_{V\text{-}SMOW}$‰	Proposed temperature	$\delta^{18}O_{H2O}$‰
Skarnoid	HTP08-52	Hetaoping 36 # adit	Banded sphalerite-rich sulfide ore with minor chalcopyrite in skarnization limstone with quartz vein	Quartz	−109	10.8	167	−3.3
Massive sulfide ore	HTP08-11	Hetaoping 88 # adit	Massive sphalerite–chalcopyrite ore and chalcopyrite rich quartz vein	Quartz	−107	11.7	156	−3.3
Massive sulfide ore	HTP08-115	Hetaoping 50 # adit	Massive sphalerite and quartz vein	Quartz	−91	12.1	235	2.3
Disseminated sulfide ore	HTP08-177	Ore heap in Hetaoping mineral processing plant	Dissemianted sphalerite–galena ore and quartz vein in marbleized limestone	Quartz	−105	10.5	158	−4.3
Quartz vein	HYA08-14	1960 adit in Heniuao ore district	Quartz vein with no minerlization	Quartz	−97	12.6	169	−1.3

Proposed temperatures are based on micothermometric data; $\delta^{18}O_{H2O}$ of ore-forming fluid was calculated based on the quartz–H_2O oxygen isotope fractionation equation of Zheng (1993).

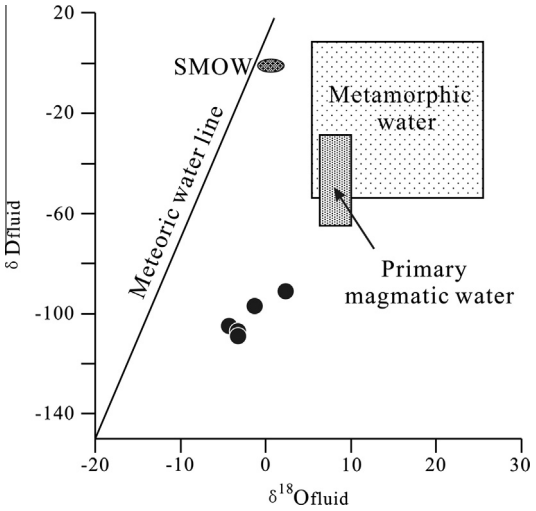

Fig. 7. Plot of δD versus $\delta^{18}O$ for fluids from the Hetaoping deposit. The fields showing the δD–$\delta^{18}O$ space occupied by metamorphic and magmatic water are after (Taylor, 1992).

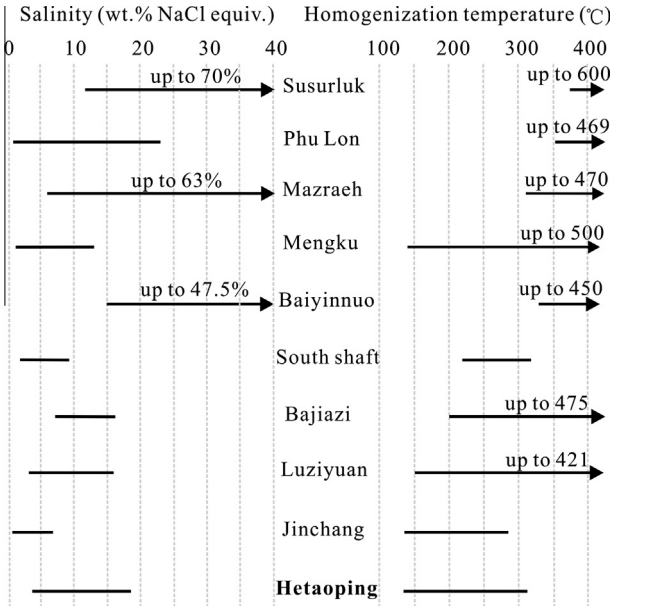

Fig. 8. Salinity and temperature data for fluid inclusions found from the Hetaoping deposit compared with fluids found in other skarn deposits.

formation of the Hetaoping skarn deposit may have been derived from a concealed intrusion.

6.2. Significance of fluid inclusions homogenization temperatures and salinities

The salinity of magmatic fluids coves a wide range (Beane, 1983) (Fig. 9). Primary magmatic fluids consist of a vapor phase with a salinity of 1–10% NaCl equivalent and a liquid phase with dozens of percent NaCl equivalent. The lower salinity vapor, the primary magmatic vapor, may form a highly saline secondary magmatic liquid after condensation accompanied by low salinity secondary magmatic vapor (Ahmad and Arthur, 1980). Average temperatures and salinities for hydrothermal fluids are shown in Fig. 9. The highly saline magmatic fluid can boil if pressure is released. This vapor can form a vapor-rich saline fluids of its own or it can be diluted by meteoric water resulting in a lower temperature and lower salinity secondary fluids. Metamorphic fluids have resulted from dehydration during the metamorphism and the compositions of these fluids are in part controlled by the protolith and the composition of other fluids that may be present, fluids like meteoric water. These fluids may have broad ranges of both temperature and salinity (Orhan et al., 2011; also see Fig. 9). In nature, the majority of hydrothermal fluids are believed to have originated from multiple fluid sources and complex fluid interactions rather than solely from fluid end-members (White, 1968; Meinert et al., 2005; Orhan et al., 2011).

In Fig. 9, all the homogenization temperatures and salinities for fluid inclusion data from Stages I and II are clustered in the same field. These points lie on the mixing lines between secondary magmatic waters and meteoric waters and they tend to fall towards the isotopically light end of the meteoric water values. This suggests that mixing between secondary magmatic water and meteoric water has taken place. In addition, some individual points from the Stage I and Stage II inclusions and all the data points from Stage III inclusions plot below the mixing area. This suggests that a large amount of meteoric water diluted the secondary magmatic component. The change of conditions involved mixing among different fluid sources would very likely cause precipitation of Pb, Zn, and other elements and could conceivably cause the formation of an ore deposits (Ahmad and Arthur, 1980; Wilkinson, 2001).

Using the data we collected and the MacFlincor computer program of Brown and Hagemann (1995), we estimate the depth of formation of Hetaoping V1 ore deposit to be 2–3 km.

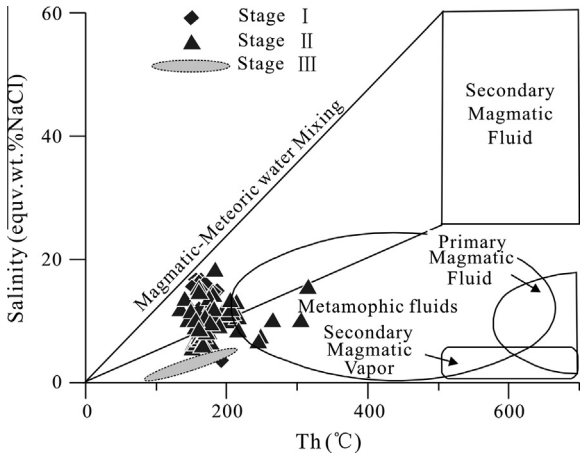

Fig. 9. Plot of homogenization temperature versus salinity for fluid inclusions from the Hetaoping skarn deposit and the average homogenization temperature–salinity distributions for hydrothermal solutions (from Beane, 1983).

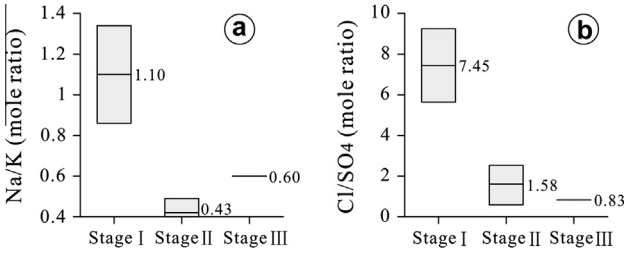

Fig. 10. Na/K (a) and Cl/SO_4 (b) ratios for fluid inclusions from Stages I–III of the Hetaoping deposit.

Table 4
Na/K and Cl/SO_4 ratios of different groups of natural waters and fluid inclusions.

Various nature waters and fluid inclusions		Average Na/K ratios	Average Cl/SO_4 ratios
Connate waters (Graf et al., 1966)	Illinois basin	249	215
	Michigan basin	94.6	757
Sea water (Sawkins, 1968)		49	19.5
Acid SO_4–Cl type volcanic waters (White et al., 1963)		13.1	3.9
Fluid inclusions (this study)		0.65	3.15

6.3. Implications of a concealed intermediate-acid intrusion

As a class, zinc skarn deposits are related to many different kinds of igneous rocks, rocks with compositions ranging from diorite to high silica granite (Meinert et al., 2005). There are no outcrops of any of these types of rocks in the Hetaoping ore area, but, as previously mentioned, geophysical surveys suggest the existence of a concealed acid-intermediate pluton in the subsurface. There has been no exploration of this hypothetical intrusion and there are on samples. Therefore in the present study we speculate on the composition of this intrusion only by comparison with other manganese skarn deposits (Meinert, 1987; Shimizu and Iiyama, 1982; Yun and Einaudi, 1982). It is notable that the intrusions related to manganese-rich skarn deposits are commonly poor in sodium and some are potassium-rich granites or diorite porphyries. Based on the comparison of these deposits with other skarn deposits of the same kind, it could be suggested that the concealed intermediate-acid intrusion associated with the deposit of the Hetaoping region may be alkaline rock.

6.4. Fluid inclusion Na/K and Cl/SO_4 ratios

A comparison of molar Na/K ratios of fluids from inclusions to that ratio for different groups of natural waters is shown in Table 4. This table shows that Na/K ratios of connate waters are by far higher than ratio in sea water (Na/K = 49), whereas the reverse is true for volcanic spring waters and fluid inclusions fluids. In addition, some connate waters are characterized by low Na/K ratios (Na/K = 5.4), which may be attributed to evaporites around the ore district (Sawkins, 1968). It is clear that Na/K ratios of the fluid inclusions in the Hetaoping deposit are more similar to volcanic spring waters than they are to connate water. Possible reasons of the low Na/K ratios in the Hetaoping fluid inclusions could include evaporites around the Hetaoping ore district or potassium-rich minerals like K feldspar or sericite with which the fluid equilibrated (Ahmad and Arthur, 1980; Sawkins, 1968). However, there are no evaporites in the Hetaoping district and therefore the low Na/K ratios of ore-forming fluids may have resulted from interaction with a deep alkaline intermediate-acid intrusion rather than evaporates. Moreover, Na/K ratios of fluids, as noted by Sawkins (1968) and by White (1968), are proportional to temperatures and we have also this relationship in our data. Our main ore stage fluids have a higher and more widespread range of Na/K ratios than the other two stages (Fig. 10a), reflecting a higher and more widespread range of temperatures.

The Cl/SO_4 molar ratios for fluids from inclusions and different groups of natural waters are also shown in Table 4. These ratios also clearly demonstrate the differences between fluid inclusions and on the one hand and connate waters and sea waters on the other. Moreover, these data also show that fluid inclusions resemble acid SO_4–Cl type volcanic waters. This again and also suggests that a genetic relationship between ore-forming fluids and volcanic waters exists as did the Na/K ratios just described. Also, note that our fluid inclusion data show that there is clearly a significant decrease in the Cl/SO_4 ratio from Stage I to Stage III (Fig. 10b), and by Stage III the Cl/SO_4 ratio has decreased to a minimum. This implies that more sulfate is in the solution and is not being precipitated from the solution to form sulfide minerals.

6.5. Geochemical and geological synthesis

There is an ongoing debate about the origin of the ore-forming fluids in the Hetaoping region. Studies on stable isotopes (C, O, H and S) and fluid inclusions of the Hetaoping Pb–Zn deposit have fostered three different camps each advocating a different source for the ore-forming fluid. The different hypotheses are: (1) mixing of magmatic water with meteoric water (Xue et al., 2008; Xue et al., 2011), (2) magmatic water (Dong and Chen, 2007), and (3) volcanic hydrothermal water (Li et al., 2006). These different viewpoints have not been resolved due to the scarcity of systematic studies on fluid inclusions. Fluid inclusions can constrain the origin of the fluids, the nature of the mineralizing water, and the genetic model (Wilkinson, 2010).

Fluid inclusions and chromatography data from different stages of orebody development in combination with hydrogen and oxygen isotope data indicate that the deposit was produced by mixing of two end member fluids—a secondary magmatic water and meteoric water. This conclusion is consistent with the geological features of the ore deposit that can be observed in the field. Two major north–northeast striking faults (the Nujiang and Lancangjiang faults) are boundary faults of the Baoshan terrane. Four groups of faults (south–north striking, northeast striking, northwest striking, and nearly east–west striking) occur throughout the region. These faults could serve as conduits for fluids rising from depth and could be interpreted as a self-organization system (Wilkinson, 2010). First, manganese-rich ore-forming fluids derived from a

deep alkaline intrusion ascended along the north–northeast striking faults to the site of carbonate host rock and interacted with the host rock. Subsequently, meteoric water also penetrated into this system though regional faults. Mixing of these fluids, especially at the fluid flow fronts, occurred and the enclosing host rocks were extensively fractured. The combination of these processes over a long period formed a positive feedback loop for a continuous process and this not only resulted in an abundance of manganese skarn minerals and sulfides but controlled the formation of the Pb–Zn skarn deposits in the Hetaoping.

7. Conclusions

Microthermometric and chromatographic data from fluid inclusions, in combination with hydrogen and oxygen isotope data, allow some important conclusions about ore deposits in the Hetaoping district to be drawn:

(1) Fluid inclusions in the pre-ore stage display low homogenization temperatures and high salinities (151–192 °C; 3.7–16.7 wt% NaCl equiv.) whereas, fluid inclusions in the main ore stage show higher homogenization temperatures and lower salinities (134–315 °C; 5.7–18.6 wt% NaCl equiv.). Fluid inclusions in the post-ore stage record lower homogenization temperatures and salinities (85–214 °C; 0.5–5.4 wt% NaCl equiv.). These data suggest that the fluid present prior to the main ore forming stage was magmatic fluid whereas the post-ore fluid was meteoric water.

(2) Based on results of the chromatography data, the fluids preserved in the Hetaoping inclusions have lower Na/K and Cl/SO_4 ratios. These ratios are similar to the ratios observed in volcanic spring waters and suggest the possibly that Hetaoping waters experienced exchange with a concealed alkaline intrusion. Higher Cl/SO_4 ratios in some Hetaoping waters suggests that, in the late stages of the ore forming process, more sulfate was in solution and was not being precipitated out of solution to form sulfide minerals. The ore-forming fluids in the Hetaoping ore district were H_2O–CO_2–N_2–CaCl type fluids.

(3) Salinities and homogenization temperatures from the three stages in the Hetaoping Pb–Zn deposit indicate that fluid mixing between magmatic water and meteoric water occurred. Higher-temperature higher-salinity fluids correspond to magmatic fluids, lower-temperature lower-salinity fluids represents meteoric waters. The hydrogen and oxygen isotope data also suggest that the ore-forming fluids were generated by mixing between magmatic fluids and some external fluids, probably meteoric waters.

Finally, manganese skarns in the Hetaoping ore district can be used as a prospecting guide. It should be mentioned that the mechanism of Pb–Zn skarn deposits genesis can be determined by analyzing the concentration of trace elements using laser ablation ICP-MS and conclusions acquired during this study need to be tested further with this analytical method.

Acknowledgements

This research project was jointly supported by the National Natural Science Foundation of China (No. 41173063), the 12th Five-Year Plan Project of State Key Laboratory of Ore-deposit Geochemistry, Chinese Academy of Sciences (SKLODG-ZY125-02) and the Knowledge Innovation Program of the Chinese Academy of Sciences (Grant Nos.: KZCX2-YW-136-2 and KZCX2-YW-111-03). We are greatly indebted to Chief Engineer Zhou Yunman (Yunnan Geology and Mineral Resources Ltd.) who assisted with sampling.

Appendix A. Supplementary material

Supplementary data associated with this article can be found, in the online version, at http://dx.doi.org/10.1016/j.jseaes.2013.04.036. These data include Google maps of the most important areas described in this article.

References

Ahmad, S.N., Arthur, W.R., 1980. Fluid inclusions in porphyry and skarn ore at Santa Rita, New Mexico. Economic Geology 75, 229–250.
Allen, V.T., Fahey, J.J., 1953. Rhodonite, johannsenite, and ferroan johannsenite at Vanadium, New-Mexico. American Mineralogist 38, 883–890.
Baertschi, P., 1976. Absolute ^{18}O content of standard mean ocean water. Earth and Planetary Science Letters 31, 341–344.
Beane, R.E., 1983. Magmatic–meteoric water transition. Geothermal Resource Council. Special Report No. 13, pp. 245–253.
Bodnar, R.J., 1993. Revised equation and table for determining the freezing point depression of H_2O–NaCl solutions. Geochimica Cosmochimica Acta 57, 683–684.
Brown, P.E., Hagemann, S.G., 1995. McFlincor and its application to fluids in Archean lode gold deposits. Geochimica Cosmochimica Acta 59, 3943–3952.
Chen, Y., Lu, Y., Xia, Q., 2005. Geochemical characteristics of the Hetaoping Pb–Zn deposit, Baoshan, Yunnan, and its genetic model and ore prospecting model pattern. Geology in China, 90–99 (in Chinese with English abstract).
Chen, Y., Huang, J., Lu, Y., 2009. Geochemistry of elements, sulphur–lead isotopes and fluid inclusions from Jinla Pb–Zn–Ag poly-metallic ore field at the joint area across China and Myanmar border. Earth Science (Journal of China University of Geosciences), 585–594 (in Chinese with English abstract).
Clayton, R.N., Mayeda, T.K., 1963. The use of bromine pentafluoride in the extraction of oxygen from oxides and silicates for isotopic analysis. Geochimica et Cosmochimica Acta 27, 43–52.
Craig, H., 1961. Standards for reporting concentrations of deuterium and oxygen 18 in natural waters. Science 133, 1833–1834.
Dong, W., 2007. The metallogenetic conditions and typical model in Baoshan–Zhenkang massif. Yunnan Geology 6, 56–61 (in Chinese with English abstract).
Dong, W., Chen, S., 2007. The characteristics and genesis of Luziyuan Pb–Zn deposit, Zhenkang. Yunnan Geology, 404–410 (in Chinese with English abstract).
Graf, D.L., Meents, F.W., Friedman, I., Shimp, N.F., 1966. The origin of saline formation waters III: Calcium chloride waters:Illinois State. Geol. Surv. Circular 397, 60p.
Kamvong, T., Zaw, K., 2009. The origin and evolution of skarn-forming fluids from the Phu Lon deposit, northern Loei Fold Belt, Thailand: evidence from fluid inclusion and sulfur isotope studies. Journal of Asian Earth Sciences 34, 624–633.
Karimzadeh Somarin, A., Moayyed, M., 2002. Granite- and gabbrodiorite-associated skarn deposits of NW Iran. Ore Geology Reviews 20, 127–138.
Li, W., Mo, X., 2001. The cenozoic tectonics and metallogenesis in the "three-river" area of southwest China. Yunnan Geology, 333–346 (in Chinese with English abstract).
Li, W., Li, L., Zhao, R., 1985. On the sedimentary ore-forming factors of the Pb–Zn deposit at Mengxing, Longling county. Yunnan Geology 4, 235–244 (in Chinese with English abstract).
Li, Z., Zeng, P., Fu, D., 2006. Geological characteristics and primary research on the genesis of the deposits in Hetaoping mineralization-concentrated region. Journal of East China Institute of Technology 29, 211–215 (in Chinese with English abstract).
Li, J., Xue, C., Wang, Y., Dong, X., Jin, J., 2011. A study on vertical zone of the Hetaoping Pb–Zn deposit in Baoshan area, Yunnan. Science and Technology and Engineering 11, 3894–3898 (in Chinese with English abstract).
Logan, M., Amelia, V., 2000. Mineralogy and geochemistry of the Gualilán skarn deposit in the Precordillera of western Argentina. Ore Geology Reviews 17, 113–138.
Meinert, L.D., 1987. Skarn zonation and fluid evolution in the Groundhog mine, Central mining district, New Mexico. Economic Geology 82, 523–545.
Meinert, L.D., Dipple, G.M., Nicolescu, A.S., 2005. Word skarn deposits. In: Economic Geology 100th Anniversary Volume. Society of Economic Geologists, Inc., pp. 299–336.
Moura, A., 2008. Metallogenesis at the Neves Corvo VHMS deposit (Portugal): a contribution from the study of fluid inclusions. Ore Geology Reviews 34, 354–368.
Orhan, A., Mutlu, H., Fallick, A.E., 2011. Fluid infiltration effects on stable isotope systematics of the Susurluk skarn deposit, NW Turkey. Journal of Asian Earth Sciences 40, 550–568.
Rao, T., 2008. Basical characteristics of lead–zinc mineral resources and the vista on geological prospecteing of super large scale lead–zinc deposits in Yunnan. China Mining Magazine 17, 108–110 (in Chinese with English abstract).

Sawkins, F.J., 1968. The significance of NaK and Cl SO_4 ratios in fluid inclusions and subsurface waters, with respect to the genesis of Mississippi Valley-type ore deposit. Economic Geology 63, 935–942.
Shimizu, M., Iiyama, J.T., 1982. Zinc–lead skarn deposits of the Nakatatsu mine, central Japan. Economic Geology 77, 1000–1012.
Tao, Y., Hu, R., Zhu, F., 2010. Ore-forming age and geodynamic background of the Hetaoping lead-zinc deposit in Baoshan Yunnan. Acta Petrologica Sinica 26 (6), 1760–1772 (in Chinese with English abstract).
Taylor, H.P., 1992. Oxygen and hydrogen isotope relationships in hydrothermal deposits. In: Barnes, H.L. (Ed.), Geochemistry of Hydrothermal Deposits, 3rd ed. John Wiley and Sons, Inc., New York, pp. 229–302.
Van den Kerkhof, A.M., Hein, U.F., 2001. Fluid inclusion petrography. Lithos 55, 27–47.
Vennemann, T.W., O'Neil, J.R., 1993. A simple and inexpensive method of hydrogen isotope and water analyses of minerals and rocks based on zinc reagent. Chemical Geology (Isotope Geoscience Section) 103, 227–234.
White, D.E., 1968. Environments of generation of some base-metal ore deposits. Economic Geology 63, 301–335.
White, D.E., Hem, J.D., Waring, G.A., 1963. Data of geochemistry Chapter F-Chemical composition of subsurface waters: U. S. Geological Survey Prof. Paper 440-F
Wilkinson, J.J., 2001. Fluid inclusions in hydrothermal ore deposits. Lithos 55, 229–272.
Wilkinson, J.J., 2010. A review of fluid inclusion constraints on mineralization in the Irish ore field and implications for the genesis of sedimented-hosted Zn–Pb deposits. Economic Geology 105, 417–442.
Xia, Q., Chen, Y., Lu, Y., 2005. Geochemistry, fluid inclusion, and stable isotope studies of Luziyuan Pb–Zn deposit in Yunnan Province, Southwestern China. Earth Science (Journal of China University of Geosciences), 177–186 (in Chinese with English abstract).
Xu, Q., Mo, X., 2000. Regional fluid characters and regimes of "Sanjiang" middle belt during Neo-Tethys. Acta Petrologica Sinica, 639–648 (in Chinese with English abstract).
Xu, L., Mao, J., Yang, F., Daniel, H., Zheng, J., 2010. Geology, geochemistry and age constraints on the Mengku skarn iron deposit in Xinjiang Altai, NW China. Journal of Asian Earth Sciences 39, 423–440.
Xue, C., Han, R., Yang, H., 2008. Isotope geochemical evidence for ore-forming fluid resources in Hetaoping Pb–Zn deposit, Baoshan, northwestern Yunnan. Mineral Deposits, 243–252 (in Chinese with English abstract).
Xue, C., Han, Y., Huang, Q., Li, J., Dong, X., 2011. Genesis and mineragenetic epoch of the Hetaoping Pb–Zn deposit in Baoshan area, Yunnan: a remote skarn-hydrothermal deposit. Acta Mineralogica Sinica, 415–418 (in Chinese with English abstract).
Yang, D., Xu, W.Y., Cui, Y.H., Chen, W.S., Lian, Y., 2007. Determination of gaseous components in fluid inclusion samples by two-dimensional gas chromatography. Rock and Mineral Analysis 26, 451–454 (in Chinese with English abstract).
Ye, L., Cook, N.J., Ciobanu, C.L., 2011. Trace and minor elements in sphalerite from base metal deposits in South China: a LA-ICPMS study. Ore Geology Reviews 39, 188–217.
Yun, S., Einaudi, M.T., 1982. Zinc–lead skarns of the Yeonhwa-Ulchin district, South Korea. Economic Geology 77 (4), 1013–1032.
Zaw, K., 2003. Geology and sulfur isotope implications of Bawdwin deposit, Northern Shan State, Myanmar: an Ag-rich, volcanic-hosted, polymetallic massive sulphide deposit. Mineral Exploration and Sustainable Development 1 and 2, 217–220.
Zhang, W., 1990. Petrogenetic mechanism and mineralization granite in Yunlong tin mining area, western Yunnan. Journal of Kunming Institute of Technology 15 (6), 1–8 (in Chinese with English abstract).
Zhang, D., Lei, Y., Luo, T., 1992. Mineralization zoning and flow direction of ore fluid in the Baiyinnuo lead–zinc deposit. Mineral Deposits, 203–212 (in Chinese with English abstract).
Zhao, Y., 1997. Metasomatic zoning in some major Pb–Zn polymetallic skarn deposits of China. Mineral Deposits, 25–34 (in Chinese with English abstract).
Zhao, Y., Dong, Y., Li, D., Bi, C., 2003. Geology, mineralogy, geochemistry, and zonation of the Bajiazi dolostone-hosted Zn–Pb–Ag skarn deposit, Liaoning Province, China. Ore Geology Reviews 23, 153–182.
Zheng, Y., 1993. Calculation of oxygen isotope fractionation in anhydrous silicate minerals. Geochimica et Cosmochimica Acta 57, 1079–1091.
Zhu, Y., Han, R., Xue, C., 2006. Geological character of the Hetaoping lead zinc deposit of Baoshan, Yunnan Province. Mineral Resources and Geology, 32–35 (in Chinese with English abstract).